Materials Research Proceedings 28 (2023) 727-736 https://doi.org/10.21741/9781644902479-79

Influence of process parameters and process set-up on damage evolution during stretch drawing of u-shaped profiles

MÜLLER Martina[1,a *], WEISER Ingo Felix[1,b], HERRIG Tim[1,c] and BERGS Thomas[1,2,d]

[1]Laboratory for Machine Tools and Production Engineering WZL of RWTH Aachen University, Campus-Boulevard 30, 52074 Aachen, Germany

[2]Fraunhofer Institute for Production Technology IPT, Steinbachstr. 17, 52074 Aachen, Germany

[a]martina.mueller@wzl.rwth-aachen.de, [b]f.weiser@wzl.rwth-aachen.de, [c]t.herrig@wzl.rwth-aachen.de, [d]t.bergs@wzl.rwth-aachen.de

Keywords: Damage, Stretch Drawing, Dual Phase Steel

Abstract. The damage state in the form of voids and lattice defects of a sheet metal component has a substantial impact on the performance of a component in service regarding fatigue or crash behaviour. Therefore, managing the damage evolution during forming, especially the accumulation and distribution of damage, by targeted changes of the process parameters and set-up enables to improve component performance by influencing the stress-strain state [1]. The evolution of the stress-strain state during the forming process and along the process route represents the most significant factor influencing the resulting damage state. This paper focuses on the influence of the damage state of sheet metal components in order to improve the performance of a component regarding fatigue and crash behavior. Considering a variation of the process parameter (drawing die radius) and change in process set-up (singlestep, multistep, reverse stretch drawing) the damage accumulation and distribution within the component is analyzed using a calibrated LEMAITRE damage model. For the consideration of this paper, an u-shaped geometry of dual phase steel DP800, which is often found as an element in vehicle body construction, is used.

Introduction

The automotive sector is one of the main contributors to CO_2 emissions [1]. Due to the climate goals of the European Union to become a net zero greenhouse gas emitting economy by 2050 [2], it is necessary to rethink the approaches in this sector and to find a way to significantly reduce CO_2 emissions. One approach is lightweight design [3]. Lightweight design enables to reduce CO_2 emissions in every life cycle by means of resource efficiency.

Stretch drawing, often combined with deep drawing, is one of the most important processes for the production of three-dimensional sheet metal components and is used in particular in the manufacturing of vehicle bodies in the automotive sector [4]. Since 40% of the total mass is attributed to the vehicle body, stretch drawing is a lever for saving CO_2 by implementing lightweight design measures [5]. One possibility to introduce lightweight design measures in stretch drawing is to reduce the thickness of the sheet metal in order to save weight. In the automotive industry in particular, however, the components used have to meet stringent requirements in order to ensure the safety of passengers in the best possible way [6].

In the field of lightweight design, high-strength materials or topology optimization are currently used in order to save material and thus weight [7]. What is currently only insufficiently exploited are the possibilities offered by the control of ductile damage along the process chain and by ductile damage meaning *the formation, growth and coalescence of voids in the microstructure. These voids are formed in structural materials by decohesion at interfaces such as phase or grain*

Materials Research Proceedings 28 (2023) 727-736 https://doi.org/10.21741/9781644902479-79

boundaries and inclusions, or by the formation of new surfaces within phases or inclusions. This damage causes degradation of the performance of the corresponding component [8]. Damage control then enables either the damage accumulation or the damage distribution to be adapted by adjusting the process parameters or process set-up in such a way that components achieve a higher performance in their subsequent application or can be designed lighter [9].

On the one hand, damage development is dependent on the strain state. However, ductile damage only occurs in combination with plastic strain. On the other hand, damage is dependent on the stress state. Li has thereby shown in the context of forming that it is not sufficient to use equivalent stress alone to model damage [10]. The three-dimensional stress state in the form of the VON MISES stress σ_{vm}, the lode parameter θ and the triaxiality η must be used (Eq. 1- 3). Whereby I_1 is the first invariant of the CAUCHY stress tensor σ and J_2 and J_3 are the second and third invariants of the deviatoric stress tensor s.

$$\sigma_{vM} = \sqrt{3J_2} \tag{1}$$

$$\eta = \frac{I_1}{\sigma_{vM}} \tag{2}$$

$$L = -\left(\frac{J_3}{\sigma_{vM}}\right)^3 \tag{3}$$

Lode parameter θ and triaxiality η are proven to have an influence on the damage and in particular also on the shape of the resulting voids. While the triaxiality η has a particular effect on the size of the voids, the lode parameter θ influences the geometry of the voids. Both parameters have in common, that they cannot be measured during stretch drawing [11]. Therefore numerical or analytical modelling is necessary.

Materials and Methods

Approach. In this paper the objective is to investigate the damage development in the form of damage accumulation and distribution. For this purpose, classical stretch drawing (SD, Fig. 1a)) with different drawing die radii r_{DR} as well as multistep stretch drawing (MSSD, Fig. 1b)) and reverse stretch drawing (RSD, Fig. 1c)) are considered. The aim is to generate the same geometry on different process routes in order to identify the influence of different load paths on damage development, so that in the future the damage development can be specifically adjusted in the form of accumulation and distribution in order to achieve a higher component performance. Due to the dependence of the damage on the stress and strain states, the load paths are first analyzed in terms of the time- and location-dependent states, which requires numerical modelling performed in this work. Afterwards the load paths are correlated with damage accumulation and distribution to disclose cause effect relations.

Stretch drawing, reverse stretch drawing and multi-step stretch drawing process. In the present work, the focus is on a u-shaped geometry from DP800 dual phase steel with a sheet thickness of $s = 1.5$ mm. The punch velocity v_p was set to $v_p = 15$ mm/s and the blank holder was position controlled due to different necessary blank holder forces to prevent the sheet metal from bypassing the drawing groove. The different processes are schematically depicted in Fig. 1.

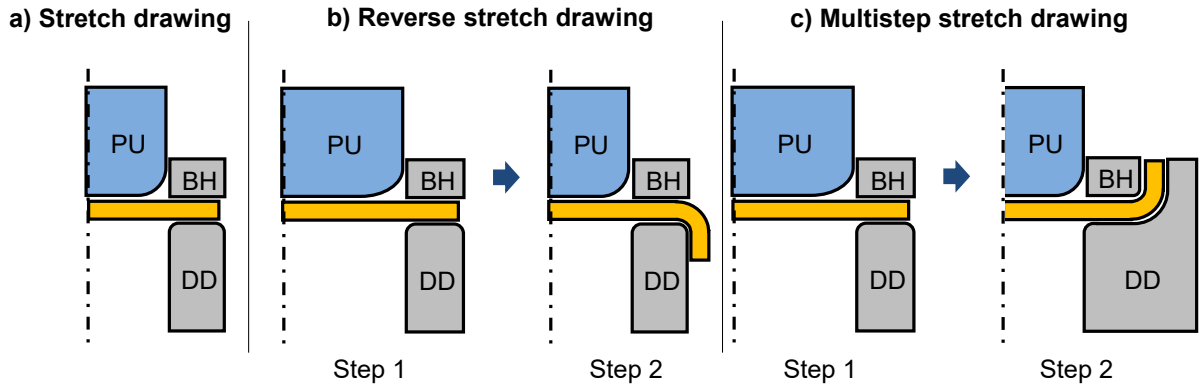

*Fig 1. SEQ Figure * ARABIC 1. Schematic illustration of a) stretch drawing, b) reverse stretch drawing and c) multistep stretch drawing.*

Process model. The SD, MSDD and RDD processes were modelled using Abaqus/explicit. To save computation time, the geometry was reduced to one quarter using symmetry. A general contact with a uniform COULOMB friction coefficient of $\mu = 0.05$ was applied to model the contact of the part, as identified in prior strip drawing tests. The parameters of the mesh as well as the types of the bodies can be seen in table 1. A LEMAITRE damage model was utilized in this paper which is based on the work of SPRAVE [12]. The model parameters of the calibrated material model are consistent with prior work [8]. The constitutive model was implemented as a VUMAT subroutine and was successfully used and validated in earlier work [13, 14].

The LEMAITRE damage model is based on the definition of the damage variable D. The parameter reflects the influence of voids and microcracks on the plastic behavior of the material [15]. The damage parameter D is defined as the ratio of the damage-free area increment ∂S and the area increment affected by damage ∂S_D (Eq. 4). As the damage grows the area increment affected by damage ∂S_D becomes greater. Thus the forces F respectively the stresses σ applied to the material are not distributed over the entire material cross section. Therefore the concept of effective stress $\tilde{\sigma}$ is introduced (Eq. 5) and used to estimate the response of the material to applied stress under consideration of damage evolution [16].

$$D = \frac{\partial S_D}{\partial S} \tag{4}$$

$$\tilde{\sigma} = \frac{\partial F}{\partial S - \partial S_D} = \frac{\sigma}{1-D} \tag{5}$$

Table 1. Parameter of the mesh and types of bodies for process model.

Name	**Mesh**	**Type of body**
Sheet	C3D8R	Solid deformable body
Punch, blank holder, die	R3D4	Discrete rigid

Reference process, reference position and area under investigation. As reference process the SD with a drawing die radius of $r_{DR} = 3$ mm is considered. The triaxiality η, lode parameter θ and damage parameter D analysis is performed at a point in the outer bend of the component (reference point (RP)), which is in principle the most sensitive area for performance in later applications. For the comparison of the die radii r_{DR}, a punch path s of $s = 25$ mm is used as reference position. This punch path s corresponds to the punch path shortly before the first component fails. For the comparison of the different process set-ups, the reference position of $s = 7.5$ mm is determined

accordingly. Due to material limitations, the process set-up only considers the area in which the components have the same geometry or have the same cup height as a functional measure of the geometry respectively.

Results

Influence of drawing die radius r_{DR} on load path and damage evolution. The damage distribution of the damage parameter D in dependence of the drawing die radius r_{DR} in the cross section of the components is shown in Fig. 2a), the course of triaxiality η and lode parameter θ in dependence of equivalent plastic strain φ_{pl} in Fig. 2b) and the course of damage parameter D in dependence of equivalent plastic strain φ_{pl} in Fig. 2c). Considering the course of the lode parameter θ as a function of the equivalent plastic strain φ_{pl} in Fig. 2b), the curves for the different die radii r_{DR} differ, in particular for the mean value ($\theta_{med.r_{DR=3}}$ =0.121, $\theta_{med.r_{DR=6}} = 0.118$, $\theta_{med.\,r_{DR=9}} = 0.116$). All curves initially start at a value of almost $\theta = 1$ and then drop and continue to progress in an oscillating manner. The course of $r_{DR} = 3$ mm, however, shows a steep peak before ending. The course of the triaxiality η, however, differs. The course of die radius r_{DR} = 3 mm of the triaxiality η has a higher value on average ($\eta_{med.r_{DR=3}} = 0.6$, $\eta_{med.r_{DR=6}} = 0.519$, $\eta_{med.r_{DR=9}} = 0.518$). Due to the non-steady shaped courses, a clear and explicit description of the courses is not possible respectively. However, what stands out concisely is the decreasing peak of $\eta_{r_{DR=3}}$ at the end. The different components also reach different equivalent plastic strains in the reference point at the reference position ($\varphi_{pl.\,r_{DR=3}} = 0.258$, $\varphi_{pl.\,r_{DR=6}} = 0.272$, $\varphi_{pl.\,r_{DR=9}} = 0.277$). The courses of the damage parameter D as a function of the equivalent plastic strain φ_{pl} in Fig. 2c) show a quadratic course with an offset with ascending drawing die radius r_{DR} for all three die radii r_{DR}. The difference in the die radius of r_{DR} = 3 mm is particularly pronounced. The damage parameter D is consistently higher for the same equivalent plastic strain φ_{pl} .

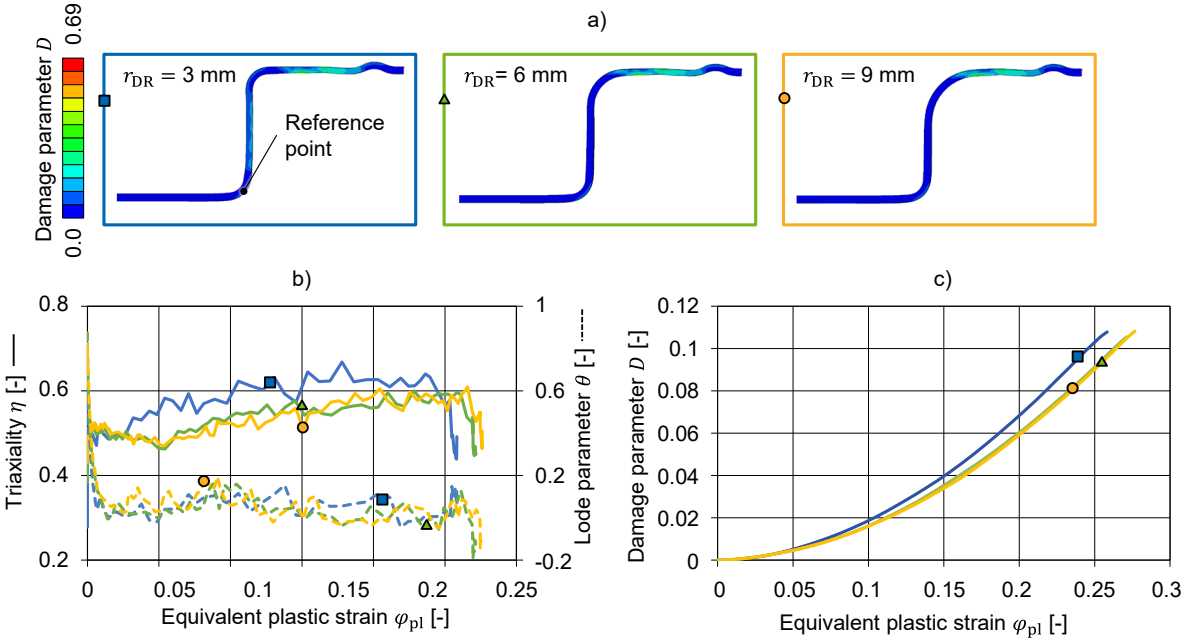

*Fig. 2. a) Damage parameter **D** distribution in cross section of components; b) course of triaxiality η and lode parameter Θ in dependence of equivalent plastic strain φ_{pl} at RP; c) course of damage parameter **D** in dependence of equivalent plastic strain φ_{pl} at RP considering different drawing die radii r_{ddr}.*

Fig. 3a) shows the course of VON MISES stress σ_{vm} in dependence of punch path s, Fig. 3b) shows the course of damage parameter D in dependence of punch path s, Fig. 3c) the damage distribution D in the cross section of the component with a drawing die radius r_{DR} = 3 mm and Fig. 3d) the course of damage parameter D in dependence of the distance x to the symmetry plane. The VON MISES stresses σ_{vm} of the individual curves all start at σ_{vm} = 0 MPa. A reverse square increase of all curves follows. With increasing die radius r_{DR}, however, a smaller gradient appears. After achieving the maximum and a slight decrease, all curves then decline to reach a quasi-stationary value to oscillate around. The drop occurs with increasing die radius r_{DR} at a later punch path s ($\sigma_{med.vM\ r_{DR}\,=\,3\ mm}$ = 806.51 MPa, $\sigma_{med.vM\ r_{DR}\,=\,3\ mm}$ = 826.98 MPa, $\sigma_{med.vM\ r_{DR}\,=\,3\ mm}$ = 832.58 MPa). The progression of the damage variable D as a function of the punch path s starts at s = 0 mm for all three curves until the first contact between blank holder and sheet and punch and sheet has been established. From a punch path of s = 2.2 mm, the curve of the die radius r_{DR} = 3 mm begins to increase, followed by the curve of the die radius r_{DR} = 6 mm and finally the curve of the die radius r_{DR} = 9 mm. Irrespective of the offset of the curves, the course of the three curves initially shows a quadratic increase, which changes to a steep linear increase and finally approaches a final value in a quadratic manner. At the reference position, the damage parameter D reaches a value of $D_{r_{DR}\,=3\ mm}$ = 0.108, $D_{r_{DR}\,=6\ mm}$ = 0.106 and $D_{r_{DR}\,=9\ mm}$ = 0.108. Considering the damage parameter D in dependence of the distance x to the symmetry plan, the three courses of the different die radii r_{DR} in the area of the wall have a nearly identical course. The same can be seen in the transition area and after the wall. In the area of the wall, in contrast, the three curves show a different course. There is a local maximum of the damage variable D with the smallest die radius r_{DR} = 3 mm. Equivalent to this is the maximum value of the damage parameter D in this area with decreasing die radius r_{DR}.

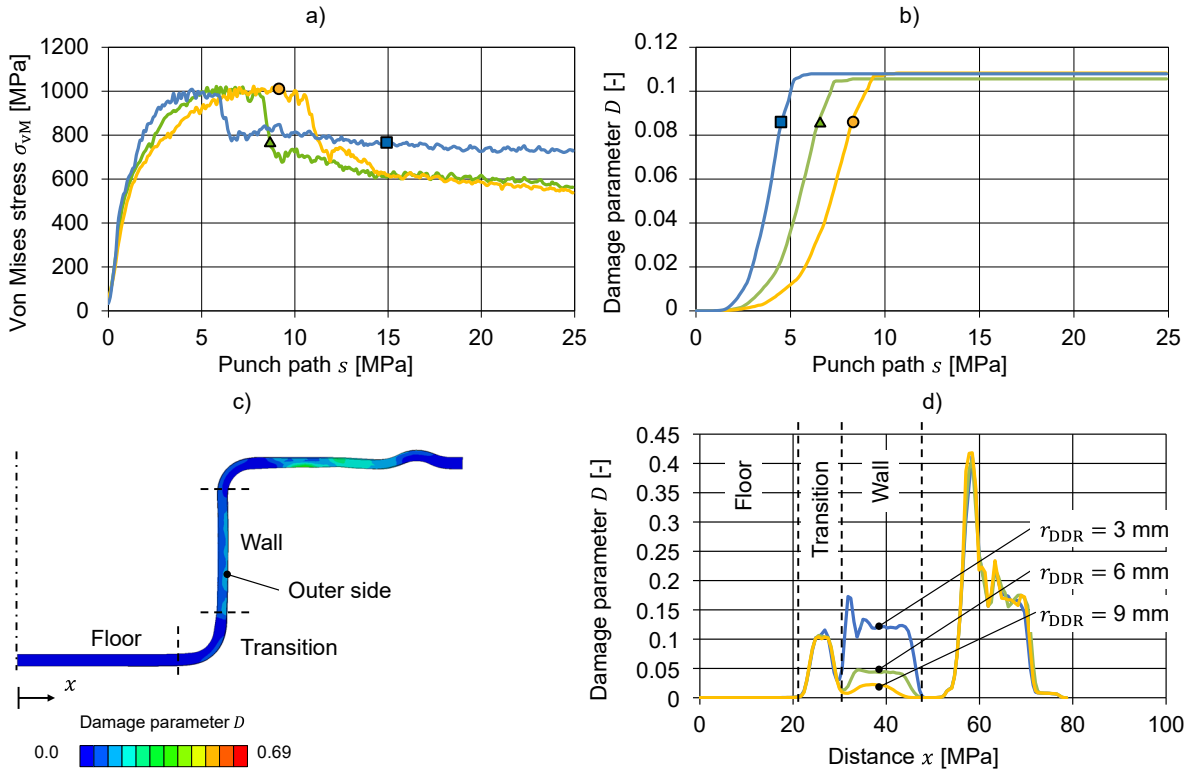

Fig. 3. a) Course of VON MISES stress σ_{vm} in dependence of punch path s at RP; b) course of damage parameter D in dependence of punch path s at RP; c) damage distribution D in cross section of component r_{DDR} = 3 mm; d) course of damage parameter D in dependence of distance x to symmetry plane considering different drawing die radii r_{ddr}.

Materials Research Proceedings 28 (2023) 727-736 https://doi.org/10.21741/9781644902479-79

Influence of process set-up on load path and damage evolution. The distribution of the damage parameter D in the cross section of the components from SD, MSSD and RSD are depicted in Fig. 4a). Considering the different heights of the cups shown in the figure, only the area up to the transition of the wall into the die radius r_{DR} was selected for the analysis of the results. This is a consequence of the fact that the maximum drawing depth was limited due to material constraints and the objective is to compare geometrically almost identical components. The courses of η_{SD}, θ_{SD} and D_{SD} are the same than in Fig. 2 since no damage respectively change of stress and strain state occurs in the reference position after a punch path of $s = 6$ mm. The damage distribution, however, differs.

The course of triaxiality η and lode parameter θ in dependence of equivalent plastic strain φ_{pl} are shown in Fig. 4b). The outer side of the outer bend, which is under consideration, experiences different equivalent plastic strains φ_{pl} to obtain the same geometry ($\varphi_{pl\,SD\,max.} = 0.26$, $\varphi_{pl\,MSSD\,max.} = 0.52$, $\varphi_{pl\,RSD\,max.} = 0.56$). The courses of the triaxiality η of MSSD and RSD show a similar behavior with mean values of $\eta_{med.MSDD} = 0.523$ and $\eta_{med.RDD} = 0.53$. Both courses start with a steep rise. After a quadratic drop, an almost linear curve follows, which drops at 0.34 and then rises again. Considering the lode parameter θ of MSDD, the course begins with a value of almost $\theta \approx 1$. The course then drops with a steep gradient into the negative range followed by an oscillating curve. This results in an average value of $\theta_{med.MSSD} = 0.21$. The course of the lode parameter θ of RSD starts similar to the course of MSDD. However, when the course drops with a steep gradient the curve remains in the positive range and starts to oscillate around a value of $\theta_{med.RSD} = 0.19$. The course of damage parameter D in dependence of equivalent plastic strain φ_{pl} considering different process set-ups is shown in Fig. 4c). The curves of MSSD and RSD depict a similar course. SD, however, has a slightly higher level of damage parameter D. The maximum value of damage parameter D obtained are $D_{MSSD} = 0.52$ and $D_{RSD} = 0.41$.

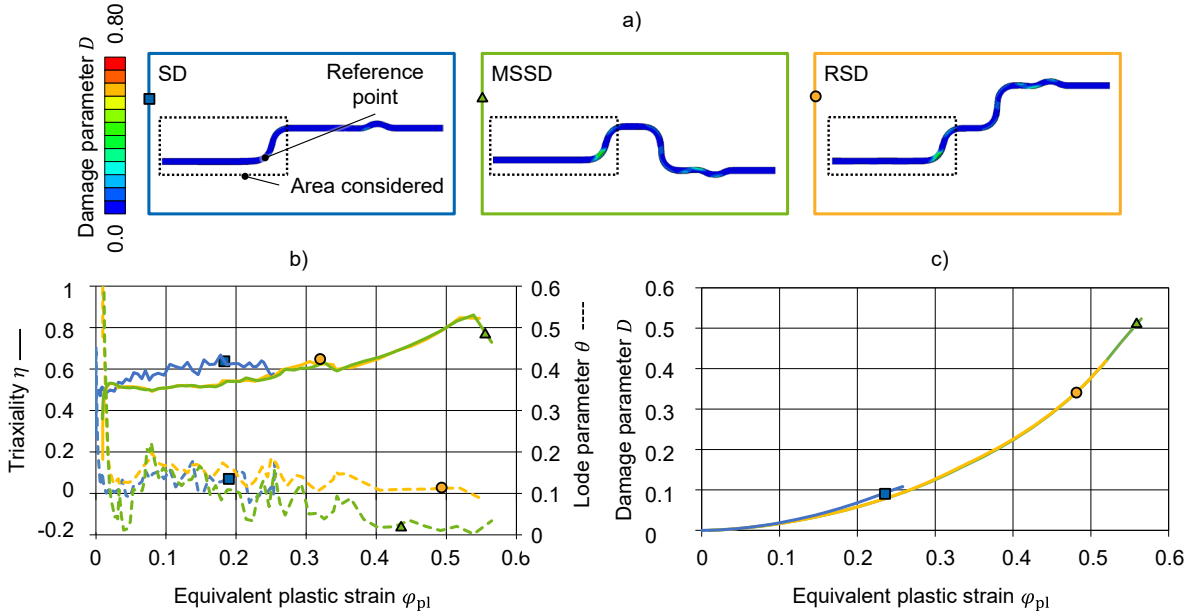

*Fig. 4. a) Damage parameter **D** distribution in cross section of components; b) course of triaxiality η and lode parameter Θ in dependence of equivalent plastic strain φ_{pl} at RP; c) course of damage parameter **D** in dependence of equivalent plastic strain φ_{pl} at RP considering different process set-ups.*

The course of VON MISES stress σ_{vm} in dependence of punch path s can be seen in Fig. 5a). The initial values of the RSD and MSSD processes differ. Since a U-profile is produced in the first step and is rotated 180° or is not rotated depending on the process route, the courses start differently. Despite the different start, both courses show a reverse square increase which is very similar. The mean values of VON MISES stress σ_{vm} obtained are $\sigma_{med.vM\ MSSD} = 882.52$ MPa and $\sigma_{med.vM\ RSD} = 852.58$ MPa. Fig. 5b) shows the course of damage parameter D in dependence of punch path s. The courses of MSSD and RSD depict a very similar quadratic course which start to elevate from a punch path s of $s = 3$ mm. The course of SD, on the other hand, shows a s-shaped course, which depicts a stronger elevation at $s = 3$ mm followed by a steady course of $D_{SD} = 0.108$. The Course of damage parameter D in dependence of distance x to symmetry plane considering different process set-ups can be seen in Fig. 5c). All three courses begin with a damage parameter $D = 0$. With the start of the transition from floor to wall, the damage parameter D increases for the first time in the courses. For MSSD and RSD, the curves show an initial quadratic rise, which changes to a linear rise with a very high gradient, and then fall off inversely. The course of SD shows a course with also a quadratic rise, but with a lower gradient as well as rise and descent shifted further to higher x values. Considering the wall of the three components, there is a small rise in damage parameter D for MSSD and RSD.

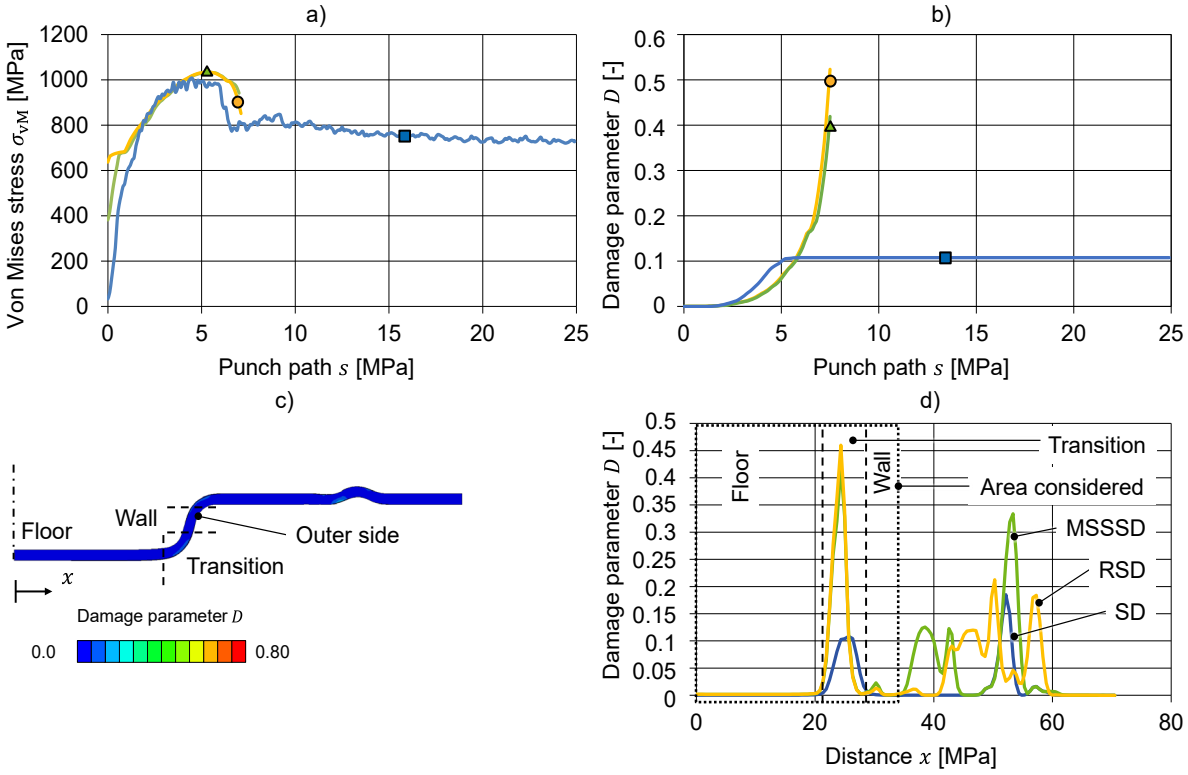

Fig. 5. a) Course of VON MISES stress σ_{vm} in dependence of punch path s at RP; b) course of damage parameter D in dependence of punch path s at RP; c) damage distribution D in cross section of component r_{DDR} = 3 mm; d) course of damage parameter D in dependence of distance x to symmetry plane mm considering different process set-ups.

Discussion

Change of die radii r_{DR}. The comparison of the load paths and the damage development at the reference point using different die radii r_{DR} shows a distinction, especially for $r_{DR} = 3$ mm. As early as from an equivalent plastic strain φ_{pl} of $\varphi_{pl} = 0.025$, a higher value of the triaxiality η

becomes apparent, which can be consulted moderately for the damage development. Analogously, the damage parameter D differs from the other two curves at the same point in strain. Due to the different equivalent strains φ_{pl} needed, however, all three achieve an almost identical damage parameter value D in the end. When observing the course of the damage parameter D as a function of the punch path s, a later onset of damage development with increasing die radius r_{DR} becomes apparent. It is concluded that this is due to the time dependent course of the bending radius of the sheet. With a smaller die radius r_{DR}, the final bending radius is reached sooner than with a higher die radius r_{DR}. Accordingly, the damage development begins at a later stage, since damage is always associated only with plastic deformation.

Considering the different equivalent plastic strains φ_{pl} at the reference point depending on the die radius r_{DR}, it is noticeable that although the bending radius is significantly smaller at $r_{DR} = 3$ mm, the equivalent plastic strain φ_{pl} is lower than with a greater die radius r_{DR}. It is assumed that the larger contact area of the sheet and the die with increasing die radius r_{DR} results in a larger frictional surface. This larger frictional surface leads to a higher flow resistance of the sheet, which results in higher punch forces. The higher punch forces required also result in higher stresses above the yield point at the reference point, which are reflected in a higher equivalent plastic strain φ_{pl}. With regard to the damage distribution in the component, it is assumed that the smaller die radius r_{DR} and the correspondingly smaller bending radius result in correspondingly higher damage parameter D in the wall of the component. This is brought into the context of greater predominant stresses in this area due to the smaller bending radius.

Change of process set-up. The course of triaxiality η of RSD and MSSD show a very similar course. The two courses differ only in the equivalent plastic strain φ_{pl} achieved. Similar to the observation of the different die radii r_{DR}, the necessary punch forces and the associated higher stresses at the reference point also seem to lead to more deformation being introduced into the area under consideration. A similar result can be seen in the course of the damage parameter D over the equivalent strain respective of the punch path s. The two curves do not differ in their characteristics, but in the final values obtained due to different equivalent strains φ_{pl}. However, severe thinning takes place in the reference position respectively the bend of the component.

Summary

A total of six different process routes for the production of a geometrically similar component were investigated. On the one hand, different drawing ring radii r_{DR} ($r_{DR} = \{3, 6, 9$ mm$\}$) and, on the other hand, different process set-ups (stretch drawing, multistep stretch drawing, reverse stretch drawing) were analyzed. The individual routes were compared with each other on the basis of their load paths and the associated damage development.

When comparing the die radii r_{DR}, a larger die radius r_{DR} at the selected reference point was found not to result in a lower damage parameter D. However, the damage development starts at a later stage with respect to the punch path s or the equivalent plastic strain φ_{pl}. Furthermore, the die radius r_{DR} was shown to have an influence on the damage distribution in the component. Particularly in the wall, a larger die radius r_{DR} resulted in less damage, which can be used for later applications to increase the performance of the component in respect of the use case. Considering the different process setups, the RSD and MSSD show very similar load paths despite different process routes, but differ in the equivalent plastic strain φ_{pl} and thus the values of the damage parameter D are different. The deformation at the reference point, however, is so severe that there is significant sheet thinning and a high damage parameter D. Due to this, the RDS and MSDD are not recommended as a suitable process route.

To complement the numerical analysis of the load paths and damage development, experimental investigations will be carried out. For this purpose, the process routes of the different die radii r_{DR} will be selected on the basis of the present results. The numerically determined load paths will then be correlated with the results regarding the damage development. Nevertheless, the present results have already enabled a pre-selection of possible process routes to be considered and the corresponding load paths to be determined.

Acknowledgements
This research was funded by Deutsche Forschungsgemeinschaft (DFG, German Research Foundation; Project number 278868966 – TRR 188; *Damage Controlled Forming Processes*). The authors would also like to thank A. Erman Tekkaya, Till Clausmeyer, Alexander Schowtjak and Jan Gerlach from the Institute of Forming Technology and Lightweight Components of TU Dortmund, sub-project S01 of TRR 188, for the usage of their implementation of the LEMAITRE damage model. Simulations were performed with computing resources granted by RWTH Aachen University under project rwth0907.

References
[1] Information on https://www.europarl.europa.eu
[2] Information on https://climate.ec.europa.eu
[3] H.J. Kim, C. McMillan, G.A. Keoleian, S.J. Skerlos, Greenhouse Gas Emissions Payback for Lightweighted Vehicles Using Aluminum and High-Strength Steel, J. Ind. Ecol. 14 (2010) 929-946. https://doi.org/10.1111/j.1530-9290.2010.00283.x
[4] F. Klocke, Manufacturing Processes: 4. Forming, Springer Berlin Heidelberg, Berlin, Heidelberg, 2013.
[5] N.P. Lutsey, Review of technical literature and trends related to automobile mass-reduction technology, University of California, Davis, 2010.
[6] Information on https://ec.europa.eu/commission/presscorner/detail/en/IP_22_4312
[7] J. Tschorn, D. Fuchs, T. Vietor, Potential impact of additive manufacturing and topology optimization inspired lightweight design on vehicle track performance, Int. J. Interact. Des. Manuf. (IJIDeM) 15 (2021) 499-508. https://doi.org/10.1007/s12008-021-00777-x
[8] M. Müller, I.F. Weiser, T. Herrig, T. Bergs, Numerical prediction of the influence of process parameters and process set-up on damage evolution during deep drawing of rectangular cups, International Conference on Accuracy in Forming Technology (ICAFT), 2022
[9] G. Hirt, E. Tekkaya, T. Clausmeyer, J. Lohmar, Potential and status of damage controlled forming processes, Prod. Eng. 14 (2020) 1-4. https://doi.org/10.1007/s11740-019-00948-6
[10] Y. Li, M. Luo, J. Gerlach, T. Wierzbicki, Prediction of shear-induced fracture in sheet metal forming, J. Mater. Process. Technol. 210 (2010) 1858-1869. http://doi.org/10.1016/j.jmatprotec.2010.06.021
[11] C.C. Roth, D.Mohr, Ductile fracture experience with locally proportional loading histories, Int. J. Plast. (2016) 328-354. https://doi.org/10.1016/J.IJPLAS.2015.08.004
[12] L. Sprave, A. Schowtjak, R. Meya, T. Clausmeyer, A.E. Tekkaya, A. Menzel, On mesh depend-encies in finite-element-based damage prediction: application to sheet metal bending, Prod. Eng. 14 (2020) 123-134. https://doi.org/10.1007/s11740-019-00937-9
[13] M. Nick, M. Müller, H. Voigts, I.F. Weiser, T. Herrig, T. Bergs, Effect of Friction Modelling on Damage Prediction in Deep Drawing Simulations of Rotationally Symmetric Cups, Defect and Diffusion Forum 414 (2022) 103-109. https://doi.org/10.4028/p-29o20d
[14] M. Nick, A. Feuerhack, T. Bergs, T. Clausmeyer, Numerical Investigation of Damage in Single-step, Two-step, and Reverse Deep Drawing of Rotationally Symmetric Cups from DP800 Dual Phase Steel, Procedia Manuf. 47 (2020) 636-642. https://doi.org/10.1016/j.promfg.2020.04.195

[15] J. Lian, Y. Feng, S. Münstermann, A modified Lamaitre Damage Model Phenomenologically Accounting for the Lode Angle 31 Effect on Ductile Fracture, Procedia Mater. Sci. 3 (2014) 1841-1847. https://doi.org/10.1016/j.mspro.2014.06.297
[16] T.S. Cao, Models for ductile damage and fracture prediction in cold bulk metal forming processes: a review, Int. J. Mater. Form. 10 (2017) 139-171. https://doi.org/10.1007/s12289-015-1262-7